This is an open access article published under an ACS AuthorChoice License, which permits copying and redistribution of the article or any adaptations for non-commercial purposes.

ACS OMEGA

Article

http://pubs.acs.org/journal/acsodf

Hybrid Cu_xO–TiO_2 Heterostructured Composites for Photocatalytic CO_2 Reduction into Methane Using Solar Irradiation: Sunlight into Fuel

Seung-Min Park,[†] Abdul Razzaq,[†] Young Ho Park,[†] Saurav Sorcar,[†] Yiseul Park,[‡] Craig A. Grimes,[§] and Su-Il In*[,†]

[†]Department of Energy Systems Engineering and [‡]Division of Nano and Energy Convergence Research, DGIST, 50-1, Sang-ri, Hyeonpung-myeon, Dalseoung Gun, Daegu 42988, Republic of Korea

[§]Flux Photon Corporation, 116 Donmoor Court, Garner, North Carolina 27529, United States

Supporting Information

ABSTRACT: Photocatalytic CO_2 conversion to fuel offers an exciting prospect for solar energy storage and transportation thereof. Several photocatalysts have been employed for CO_2 photoreduction; the challenge of realizing a low-cost, readily synthesized photocorrosion-stable photocatalytic material that absorbs and successfully utilizes a broad portion of the solar spectrum energy is as yet unmet. Herein, a mesoporous p-type/n-type heterojunction material, Cu_xO–TiO_2 (x = 1, 2), is synthesized via annealing of Cu/Cu_2O nanocomposites mixed with a TiO_2 precursor ($TiCl_4$). Such an experimental approach in which two materials of diverse bandgaps are coupled provides a simultaneous opportunity for greater light absorption and rapid charge separation because of the intrinsic p–n heterojunction nature of the material. As detailed herein, this heterostructured photocatalyst demonstrates an improved photocatalytic activity. With the CO_2 reduction of our optimal sample (augmented light absorption, efficacious charge separation, and mesoporosity) that utilizes no metal cocatalysts, a remarkable methane yield of 221.63 ppm·g^{-1}·h^{-1} is achieved.

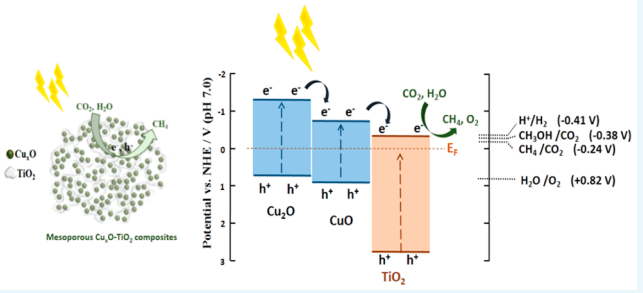

1. INTRODUCTION

The continuous increase in atmospheric CO_2 concentration is considered to be a key driver that induces climate change.[1] The prospect of unwanted climate change or climate heating–desertification has compelled investigations into the means to normalize atmospheric CO_2 concentrations. As is well known, CO_2 is a highly stable molecule, requiring significant energy input for its reduction.[2] In this regard, sunlight is considered to be the most useful energy source for promoting CO_2 conversion into useful hydrocarbon products, such as methane or ethane, offering the possibility of turning sunlight into fuels compatible with the current energy infrastructure.

During the past several decades, titanium dioxide (TiO_2) has received much attention as a photocatalyst because of its abundant availability, nontoxicity, photocorrosion resistance, and excellent charge transport properties.[3] However, the TiO_2 bandgap of 3.2 eV limits its absorption to the ultraviolet region, making it utilize only 4% of the entire solar spectrum. To reduce the TiO_2 bandgap such that it absorbs a greater portion of the solar spectrum energy while maintaining its commendable properties, various strategies have been investigated, such as anion doping,[4] loading of noble metals like Pt, Pd, Au, and so forth to act as cocatalysts,[5,6] and coupling of TiO_2 with low-bandgap semiconductors.[7] Composites of Cu_xO and TiO_2 have been utilized for hydrogen evolution,[8] CO_2 photoreduction,[9] and photodegradation of volatile organic compounds[10] and as visible light-responding photocathodes.[11] Therefore, we believe that coupling TiO_2 with a suitable low-bandgap semiconductor, our interest herein, can result in a broad-spectrum visible light-absorbing material with improved photocatalytic activities. The present hybrid photocatalyst based upon Cu_xO–TiO_2 showcases a performance better than those of the previously reported studies on CuO–TiO_2 for CO_2 photoreduction into methane.[9,12]

Herein, we report the synthesis and the photocatalytic application of a mesoporous p–n heterojunction composite material without metal cocatalyst sensitization, as commonly used. Our material is composed of p-type Cu_xO (CuO and Cu_2O) with a bandgap of ∼1.35–1.7 eV,[13] coupled with n-type TiO_2. The Cu_xO–TiO_2 photocatalyst is prepared using a facile and inexpensive two-step process: briefly, Cu/Cu_2O nanocomposites are synthesized via thermal decomposition, which are then vigorously mixed with titanium tetrachloride ($TiCl_4$) under an argon atmosphere, forming a gelatinous solution. The calcination under air of this gelatinous solution results in a mesoporous Cu_xO–TiO_2 composite.

Received: August 2, 2016
Accepted: October 24, 2016
Published: November 8, 2016

Downloaded via DAEGU GYEONGBUK INST SCI & TECHLGY on April 23, 2020 at 05:18:00 (UTC).
See https://pubs.acs.org/sharingguidelines for options on how to legitimately share published articles.

 © 2016 American Chemical Society

DOI: 10.1021/acsomega.6b00164
ACS Omega 2016, 1, 868–875

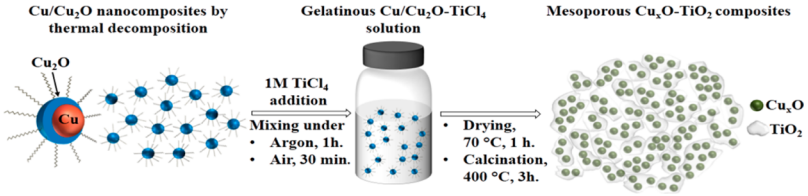

Figure 1. Schematic view of our experimental approach for the synthesis of the mesoporous Cu_xO-TiO_2 photocatalyst.

During the ambient-atmosphere calcination process, (1) $TiCl_4$ oxidizes to form TiO_2; (2) Cu/Cu_2O nanocomposites are oxidized, forming Cu_xO (CuO and Cu_2O); and (3) organic ligands used in the synthesis of Cu/Cu_2O nanocomposites are removed, providing a firm heterojunction formation between Cu_xO and TiO_2 with a well-defined mesoporous morphology. A schematic diagram showing our experimental approach is shown in Figure 1.

We test the resulting photocatalyst for its ability to promote the ambient-temperature photoconversion of CO_2 and water vapor to hydrocarbons and to discover a high rate conversion of CO_2 to, almost exclusively, methane without the use of noble metal codopants. For the purpose of optimization, various samples of Cu_xO-TiO_2 are prepared with various amounts of $TiCl_4$ (TiO_2 precursor), namely, CT03, CT05, CT07, and CT09 corresponding to 0.3, 0.5, 0.7, and 0.9 mL of $TiCl_4$, respectively, mixed with 20 mL of Cu/Cu_2O nanocomposites dispersed in toluene. To the best of our knowledge, for the first time, hybrid mesoporous p-type Cu_xO (CuO and Cu_2O) coupled with n-type TiO_2 for photocatalytic conversion of CO_2 into hydrocarbon fuels without using metal cocatalysts is introduced.

2. RESULTS AND DISCUSSION

2.1. Characterization of the Cu_xO-TiO_2 Composites.

The X-ray powder diffraction (XRD) patterns of pure CuO, pure TiO_2 (synthesized from $TiCl_4$), and Cu_xO-TiO_2 samples are shown in Figure 2.[10] The XRD patterns of the Cu_xO-TiO_2

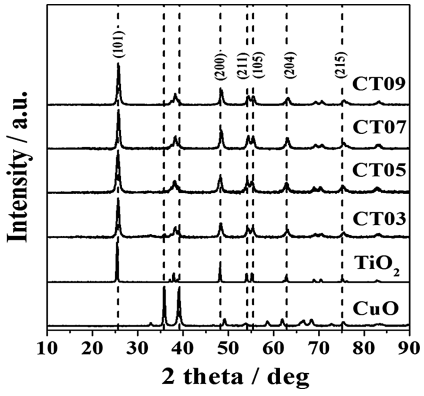

Figure 2. XRD patterns of pure CuO, pure TiO_2 and Cu_xO-TiO_2 samples.

samples mainly show, an intense peak at $2\theta = 26.2°$, corresponding to d_{101} of anatase TiO_2, confirming the presence of anatase TiO_2 as well as a relatively small amount of Cu/Cu_2O nanocomposites in the Cu_xO-TiO_2 samples. This result, we assume, is likely due to the low crystallinity and high dispersion of Cu_xO species on TiO_2 surfaces.[8,10] From the inductively coupled plasma-atomic emission spectroscopy (ICP-AES) analysis of the representative sample CT07, 2 wt % Cu is determined, which corresponds to approximately 80% of the Cu content obtained using the data from the field emission scanning electron microscopy (FE-SEM) energy-dispersive spectroscopy (EDS) technique (Figure S5).

Transmission electron microscopy (TEM) and high-resolution TEM (HR-TEM) images of the Cu/Cu_2O nanocomposites and a representative Cu_xO-TiO_2 sample (CT07) are shown in Figure 3. The as-synthesized Cu/Cu_2O

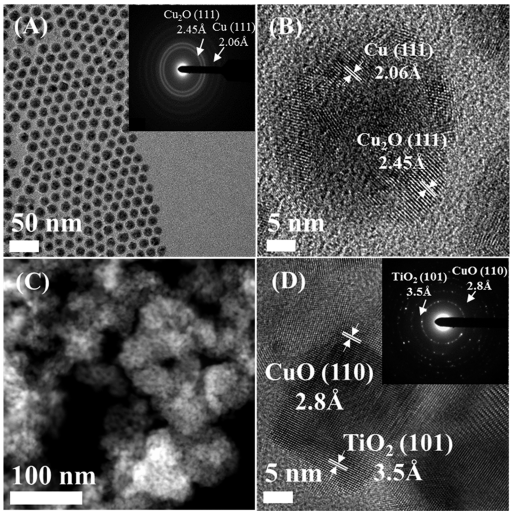

Figure 3. (A) TEM image and SAED pattern (inset) of Cu/Cu_2O nanocomposites and (B) HR-TEM image of single Cu/Cu_2O nanocomposites, (C) STEM image of the sample CT07, by which the mesoporous nature of the photocatalyst can be clearly discerned, and (D) HR-TEM and SAED patterns (inset) confirming the presence of CuO and TiO_2 within the mesoporous Cu_xO-TiO_2 composite.

nanocomposites show excellent size uniformity (Figure 3A) with the selected area electron diffraction (SAED) pattern showing d_{111} planes for both Cu_2O and Cu. The HR-TEM image (Figure 3B) shows respective lattice fringes for Cu_2O and Cu metal, which are well-matched with the SAED pattern.[10] To check the mesoporosity of the Cu_xO-TiO_2 sample, FE-SEM and HR-TEM images of the sample CT07 can be seen in Figures S2 and S3, respectively. Furthermore, the STEM image of the sample CT07 (Figure 3C) confirms the readily discernible mesoporous nature of the Cu_xO-TiO_2 samples. The STEM elemental mapping of the CT07 sample further (Figure S4) confirms the presence of Cu and Ti. Figure 3D exhibits the HR-TEM image of the sample CT07 showing well-defined lattice fringes of 0.28 and 0.35 nm, corresponding to the d_{110} plane of CuO and the d_{101} plane of TiO_2, respectively. The SAED pattern of an interface region (inset of Figure 3D) further confirms the formation of CuO and TiO_2 regions within the Cu_xO-TiO_2 matrix with rings indexed to the d_{110} plane of CuO and the d_{101} plane of anatase TiO_2.[10]

DOI: 10.1021/acsomega.6b00164
ACS Omega 2016, 1, 868−875

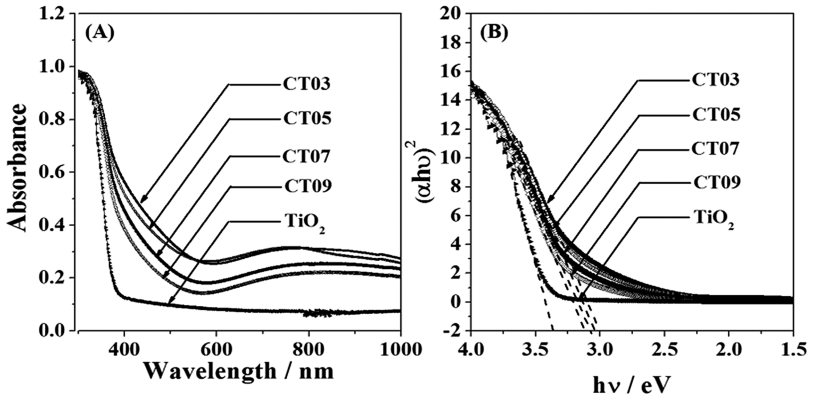

Figure 4. (A) UV−vis DRS of all samples showing red shift in the Cu_xO-TiO_2 samples attributed to the formation of a Cu_xO-TiO_2 heterojunction and absorption in the 600−1000 nm range because of Cu_xO intrinsic absorptions. (B) Corresponding Tauc plots for the bandgap estimation of the Cu_xO-TiO_2 samples.

Table 1. Photocatalytic and Textural Properties of the Cu_xO-TiO_2 Samples

sample	S_{BET}[a] ($m^2 \cdot g^{-1}$)	pore volume[b] ($cm^3 \cdot g^{-1}$)	bandgap[c] (eV)	amount of CH_4[d] ($ppm \cdot g^{-1} \cdot h^{-1}$)
CT03	11.05	0.115	3.09	23.33
CT05	16.49	0.102	3.12	55.07
CT07	26.95	0.094	3.15	221.63
CT09	22.95	0.164	3.2	168.03

[a]The surface areas of the samples are determined by using the BET equation to a relative pressure (P/P_0) range of 0.05−0.35 of the adsorption isotherm. [b]Barrett−Joyner−Halenda (BJH) equation using the desorption isotherm is used to calculate the pore volume. [c]Tauc plots are made for bandgap energy estimation. [d]Amount of CH_4 evolved is calculated using eq 7.

The UV−vis diffuse reflectance spectra (UV−vis DRS) of pure TiO_2 and Cu_xO-TiO_2 samples (Figure 4A) exhibit two prominent changes: (1) pure TiO_2 is unable to absorb visible light, whereas the UV−vis DRS spectra of the modified samples exhibit a shift in the absorption edge to longer wavelengths (400−600 nm), which is attributed to the formation of a heterojunction between Cu_xO and TiO_2;[14,15] and (2) the absorption band in the near infrared (600−1000 nm) is observed because of the Cu loading and thus is attributed to a $2E_g \rightarrow 2T_{2g}$ interband transition in the Cu^{II} clusters deposited over TiO_2.[16]

The bandgap values of all samples are estimated using Tauc plots (Figure 4B) and are listed in Table 1. The variation in the bandgap can be attributed to the amount of Cu/Cu_2O present. The bandgap of the composites gradually increases with an increase in the $TiCl_4$ content; the lowest value was 3.09 eV for sample CT03 containing 0.3 mL of $TiCl_4$ mixed in a 20 mL Cu/Cu_2O solution.

The photoluminescence (PL) spectra of TiO_2 (synthesized from the $TiCl_4$ precursor), Cu/Cu_2O nanocomposites, and the sample CT07 can be seen in Figure 5. Pure TiO_2 depicts a sharp peak around 385 nm because of emission from band-to-band recombination with other peaks appearing in the range of 400−600 nm, attributed to the electron transitions from the inter-bandgap defect levels.[17,18] Cu/Cu_2O nanocomposites exhibit a UV emission peak at 380 nm and a visible emission peak at 520 nm, attributed to the recombination of electron−hole pairs in free excitons or deep-level defects and photogenerated electrons in Cu_xO, respectively.[19,20] For the sample CT07, the visible emission peak for Cu_xO at 520 nm is quenched as compared to that of Cu/Cu_2O nanocomposites, thereby suggesting the formation of a p−n junction at the interface, resulting in a reduced rate of recombination.

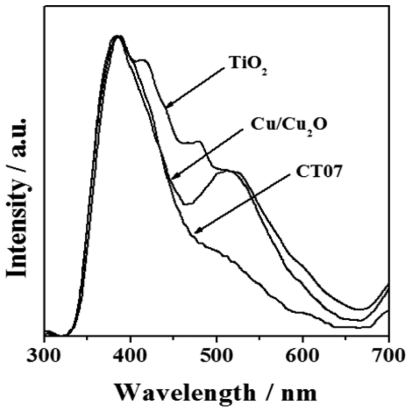

Figure 5. PL emission spectra of pure TiO_2, Cu/Cu_2O nanocomposites, and the sample CT07.

The Brunauer−Emmett−Teller (BET) surface areas and pore-size distributions are measured for all Cu_xO-TiO_2 samples (Figure S6), with their values displayed in Table 1. CT07 shows the largest surface area (26.95 $m^2 \cdot g^{-1}$), approximately 2.4 times higher than that of CT03 (11.05 $m^2 \cdot g^{-1}$). It is observed that on increasing the amount of $TiCl_4$, the surface area decreases, possibly because of the increased aggregation induced by the higher amounts of the Ti precursor.

Further evidence for Cu_xO-TiO_2 formation comes from an X-ray photoelectron spectroscopy (XPS) analysis of the sample CT07. Figure 6A shows the Ti 2p region with two intense peaks at 457.6 and 464.0 eV, corresponding to Ti $2p_{3/2}$ and Ti $2p_{1/2}$ states, respectively, ensuring the presence of Ti^{4+} ions.[21] The satellite shoulder peaks appearing at higher binding energies are assumed to be because of the Ti^{4+} state in the Ti−O−Cu structure.[22] The Cu 2p region (Figure 6B) exhibits Cu $2p_{3/2}$ and Cu $2p_{1/2}$ main peaks appearing around 933.0 and

DOI: 10.1021/acsomega.6b00164
ACS Omega 2016, 1, 868−875

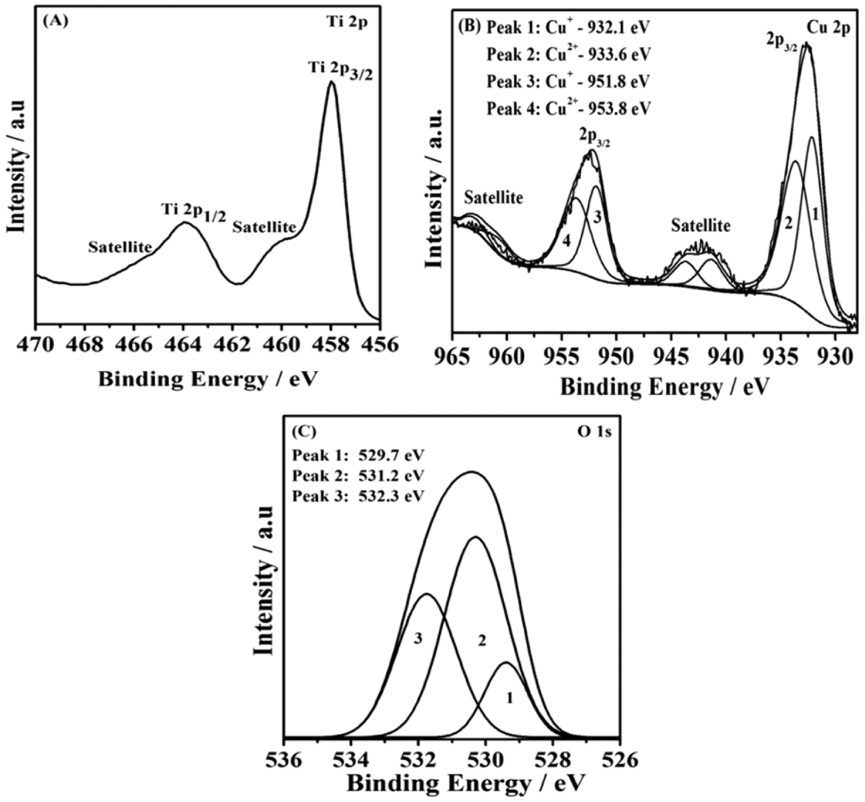

Figure 6. XPS of the sample CT07 showing (A) the Ti 2p region with characteristic Ti peaks assigned to Ti $2p_{3/2}$ and Ti $2p_{1/2}$, (B) characteristic Cu 2p peaks and satellite peaks assuring the presence of Cu_2O and CuO, and (C) the O 1s region exhibiting three peaks located at 529.7, 531.2, and 532.3 eV corresponding to Ti−O, O−H, and C−O bonds, respectively.

953.0 eV, with satellite peaks at 942.5 and 962.5 eV, respectively. The main Cu 2p peaks are further deconvoluted into four peaks, where peak 1 and peak 3 are assigned to the Cu^+ species (Cu_2O), whereas peak 2 and peak 4 are associated with the Cu^{2+} species (CuO).[14,23] The satellite peaks are attributed to the ligand-to-metal charge transfer, an important indicator of the presence of Cu^{2+} species[24] by an open 3d shell,[9] which is not observed for Cu^+ or metallic Cu^0 species because of their completely filled 3d shell.[10] Furthermore, the energy gap between peak 2 and peak 4 is 20.0 eV, which matches well with the standard value of 20.0 eV for CuO.[23] The Cu 2p XPS data suggest the presence of two phases, that is, CuO and Cu_2O in the as-prepared samples. The O 1s region (Figure 6C) reveals the presence of three peaks located at 529.7, 531.2, and 532.3 eV corresponding to Ti−O, O−H, and C−O bonds, respectively.[8] The XPS spectra of all other synthesized samples, namely, CT03, CT05, and CT09, are given in Figures S7, S8, and S9, respectively. All samples show characteristic peak positions similar to that of the representative sample CT07, confirming the successful formation of the Cu_xO−TiO_2 heterojunction.

2.2. Photocatalytic Conversion of CO_2 into Methane and Its Proposed Mechanism. Photocatalytic CO_2 conversion into hydrocarbon fuels is used to test the Cu_xO−TiO_2 sample. Pure TiO_2 (synthesized from the $TiCl_4$ precursor) and pure bulk CuO are used as reference samples. Analysis of the products obtained from all samples using gas chromatography (GC) predominantly shows methane as the main hydrocarbon product. Figure 7 shows that the methane production rate after each sample is illuminated for 1 h of solar illumination. When Cu_xO is coupled with TiO_2, all samples show an increase in the

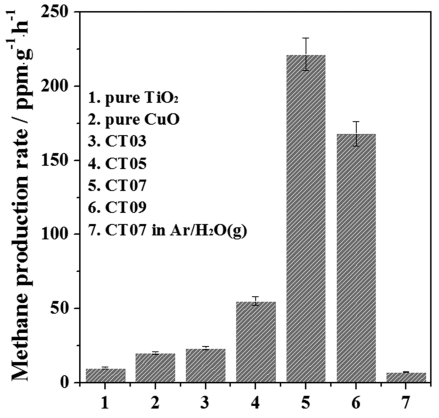

Figure 7. Rates of CH_4 evolution measured under simulated solar irradiation for pure TiO_2, pure CuO, and all Cu_xO−TiO_2 samples. The sample CT07 shows the highest methane evolution rate of 221.63 $ppm{\cdot}g^{-1}{\cdot}h^{-1}$. The control test of the CT07 sample in an $Ar/H_2O(g)$ mixture exhibits negligible CH_4 evolution.

CH_4 yield. With an increasing amount of $TiCl_4$ for the synthesis of Cu_xO−TiO_2, the amount of CH_4 evolution increases, reaching a maximum value with CT07. A further increase in $TiCl_4$ beyond CT07 decreases the CH_4 yield, which we believe is due to the low surface area of CT09 limiting active sites to interact with the CO_2 molecules. CT07 exhibits a methane evolution of 221.63 $ppm{\cdot}g^{-1}{\cdot}h^{-1}$, a value which is 11.1 times and 22 times higher than for pure CuO (20.01 $ppm{\cdot}g^{-1}{\cdot}h^{-1}$) and TiO_2 (9.94 $ppm{\cdot}g^{-1}{\cdot}h^{-1}$), respectively. It is noted that this yield is better than those of our previously reported photocatalysts utilized for CO_2 conversion into methane.[9,25−28]

DOI: 10.1021/acsomega.6b00164
ACS Omega 2016, 1, 868−875

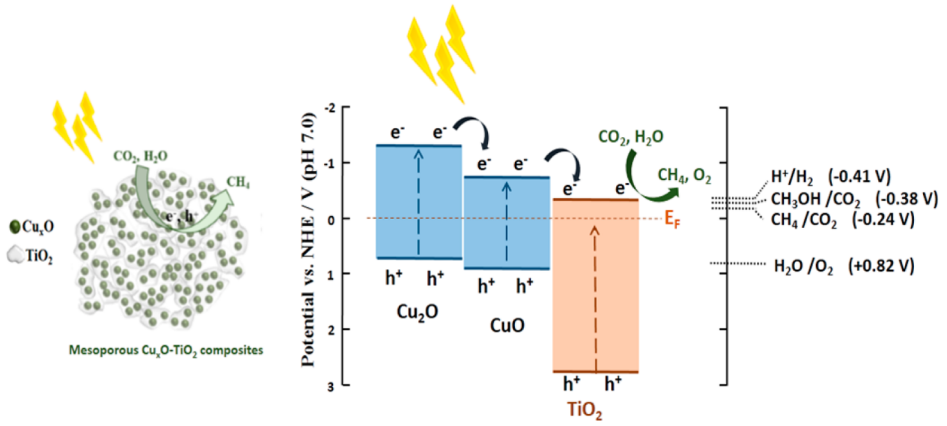

Figure 8. Schematic illustration of the photocatalytic reduction of CO_2 into CH_4 using Cu_xO-TiO_2 heterojunction samples.

The rate of CH_4 production is calculated for all Cu_xO-TiO_2 samples using eq 7, as listed in Table 1. Control tests performed by illuminating CT07 in an $Ar/H_2O(g)$ atmosphere under similar irradiation conditions show a negligible amount of CH_4 evolution. Thus, it can be inferred from the control experiment that CH_4 evolved during the normal experiments is due to the photoreduction of CO_2 and not because of the oxidation of surface-bound organics.

The stability of the representative sample CT07 is measured by its repeated testing for five cycles (Figure S11). The representative sample CT07 shows good stability without any acute decrease in the methane production rate: hence, one can see that the rate of CO_2 reduction on the fifth test is approximately 88% that of the first.

An elucidation based upon experimental results and on the literature that reported the energy levels and the suggested process for the conversion of CO_2 and water vapor into methane is shown in Figure 8. As revealed by XPS data, Cu_xO-TiO_2 contains both Cu_2O and CuO, the conduction band edges of which are both more negative than TiO_2.[29−31] Thus, upon illumination within the Cu_xO-TiO_2 photocatalyst, generation of electrons (e^-) and holes (h^+) takes place, whereby the electrons in p-type Cu_xO can easily flow to the conduction band of TiO_2 to contribute to the photoreduction of adsorbed CO_2, whereas the photogenerated holes migrate in the opposite direction to oxidize the adsorbed H_2O, releasing H^+ and O_2.

The photoreduction of CO_2 is a complex process. Initially, the adsorption of CO_2 takes place over the semiconductor surface, leading to an activation of the CO_2 molecule for reduction. Although CO_2 is a linear molecule, its adsorption on a photocatalyst surface transforms it into a bent structure, with a decrease in the lowest unoccupied molecular orbital (LUMO) level of CO_2, thus offering a lower barrier for accepting electrons under illumination.[32] When light is illuminated upon the CO_2-adsorbed photocatalytic material, the photoexcited electrons generated are injected to the adsorbed CO_2 to proceed with the reduction reactions, with the formation of various intermediate free radicals and products.[33] Among the various CO_2 photoreduction mechanisms proposed, the carbene pathway is the most widely accepted pathway for yielding CH_4 and/or CH_3OH as the main products.[33] The literature for the carbene pathway mechanism is well-defined and is considered reliable based on the investigations made using electron spin resonance (ESR) and electron paramagnetic resonance (EPR) experimental techniques.[34−36] The carbene pathway begins with the injection of a single electron into the adsorbed CO_2, forming an anion radical $CO_2^{\bullet-}$.[37] Such a single electron reduction of CO_2 to an anion radical $CO_2^{\bullet-}$ possesses a strong negative electrochemical potential of −1.9 V versus a normal hydrogen electrode (NHE).[36] Hence, with such a high potential required for this step, it seems highly improbable for the semiconductors to proceed with the reduction. Therefore, at this stage, it is considered that as soon as the $CO_2^{\bullet-}$ radical is formed, it reacts with the protons H^+ (provided by water oxidation via filling holes) and photogenerated electrons to produce intermediate radicals and products. Such a process is known as "proton-assisted multielectron reduction" and is generally acceptable for the CO_2 photoreduction process. The radicals and products produced at the intermediate stages further undergo a series of proton-assisted multielectron reductions, finally yielding CH_4 as the main product. Thus considering the proton-assisted multielectron reduction via the carbene pathway, we propose a possible route for CO_2 photoreduction, a schematic view of which is shown in Figure 8. Photogenerated electrons (e^-) and holes (h^+) are generated at the active sites of the Cu_xO-TiO_2 photocatalyst (eq 1). The holes (h^+) react with the adsorbed H_2O to produce hydroxyl radicals ($OH^\bullet$) and protons (H^+) (eq 2). The surface-adsorbed $CO_2^{\bullet-}$ radical generated by the injection of a single electron (eq 3) reacts with e^- and H^+, producing CO (eq 4), which undergoes a further reduction process forming the surface-adsorbed C (eq 5). This surface-adsorbed C reacts with $4e^-$ and $4H^+$ to yield CH_4 (eq 6) as a main product. The proposed reactions involved in the CO_2 photoreduction to CH_4 can be described by eqs 1−6.

$$Cu_xO-TiO_2 \xrightarrow{h\nu} e_{CB}^- + h_{VB}^+ \quad (1)$$

$$H_2O + h^+ \rightarrow H^+ + OH^\bullet \quad (2)$$

$$CO_2 + e^- \rightarrow CO_2^{\bullet-} \quad (3)$$

$$CO_2^{\bullet-} + e^- + H^+ \rightarrow CO + OH^- \quad (4)$$

$$CO + 2e^- + H^+ \rightarrow C + OH^- \quad (5)$$

$$C + 4e^- + 4H^+ \rightarrow CH_4 \quad (6)$$

3. EXPERIMENTAL SECTION

3.1. Synthesis of Mesoporous Cu_xO-TiO_2 Heterostructured Composites. The synthesis of mesoporous

DOI: 10.1021/acsomega.6b00164
ACS Omega 2016, 1, 868−875

Cu_xO-TiO_2 heterostructured composites was carried out using a simple impregnation step. An already prepared Cu/Cu_2O nanocomposite solution (6 mL) (details in Supporting Information) was dispersed in 20 mL of anhydrous toluene in a rubber-capped vial and degassed for 30 min under vacuum to remove any air dissolved in the solution and filled with an inert gas (Ar). The degassed solution was transferred into the glove box, followed by a dropwise addition of a certain amount of 1 M titanium(IV) chloride solution (0.3, 0.5, 0.7, and 0.9 mL of $TiCl_4$) to the degassed solution. The color of the solution changes from dark green to dark yellow. After 1 h of reaction, a well-dispersed solution mixture of dark yellow Cu/Cu_2O nanocomposite and $TiCl_4$ was formed and is allowed to oxidize spontaneously in air for 30 min under stirring. A change in the color of the mixture from dark yellow to reddish brown is observed. The gel-type mixture of Cu/Cu_2O nanocomposite and $TiCl_4$ was dried under air at 70 °C and then subsequently calcined in a tubular furnace at 400 °C, at a ramping rate of 6 °C/min under air flow (20 cc/min) for 3 h. The annealing process oxidizes both the Cu/Cu_2O nanocomposite and $TiCl_4$ forming Cu_xO-TiO_2 (where x = 1 or 2), a well-known oxidation process that has been reported earlier.[38−40] The Cu_xO-TiO_2 samples obtained with 0.3, 0.5, 0.7, and 0.9 mL of $TiCl_4$ were labeled as CT03, CT05, CT07, and CT09, respectively.[41]

3.2. Photocatalyst Characterization. XRD studies were performed using a Panalytical, Empyrean diffractometer with Cu Kα radiation (λ = 1.54 Å) in the range of 2θ = 10°−90° at 1°/min. Surface morphologies and composition were observed using a field emission scanning electron microscope (Hitachi S-4800) equipped with an EDS attachment. High-resolution images were obtained using a field emission transmission electron microscope (FE-TEM, Hitachi HF-3300) operating at 300 kV, where the samples were prepared on a Ni grid.

The surface areas of the products were analyzed using the BET method (Micromeritics ASAP 2000 apparatus) at −196 °C. XPS (Thermo VG, K-alpha) with Al Kα line operating at 148 606 eV as the X-ray source was used to study the surface composition and oxidation states of Cu_xO-TiO_2. The optical properties of the samples were studied using UV−vis DRS Cary series (Agilent Technologies) with an attached diffuse reflectance accessory. PL was measured using a Cary Eclipse fluorescence spectrophotometer (Agilent Technologies), λ_{exc} = 300 nm for all samples. The copper content in the photocatalyst was deduced using the ICP-AES analysis using a Thermo Scientific iCAP 7400 duo ICP-AES instrument.

3.3. Photocatalytic CO_2 Conversion. In the photocatalytic CO_2 conversion experiment, an empty photoreactor (stainless steel; volume = 15.4 cm^3) was purged with CO_2 gas (1000 ppm in He) and vacuum simultaneously to remove any air or other impurities before and after the loading of the photocatalyst.[41] The photocatalyst (50 mg) was loaded into the photoreactor; moist CO_2 gas (1000 ppm in He) was passed through a water bubbler, which then enters the photoreactor. The photocatalyst-loaded photoreactor, filled with a mixture of CO_2 and H_2O vapors mixture, was then illuminated by a 100 W Xenon solar simulator (Oriel, LCS-100) with an AM1.5 filter for 1 h, and the reaction products (500 μL) were analyzed using a Shimadzu GC-2014 gas chromatograph (Restek Rt-Q Bond column, ID = 0.53 mm, and length = 30 m) equipped with flame ionization (FID) and thermal conductivity (TCD) detectors. Figure S1 shows the schematic of the experimental setup for the photocatalytic CO_2 reduction. The hour-normalized photocatalytic CH_4 evolution rate is calculated using eq 7.

$$\text{Rate of } CH_4 \text{ evolution} = \frac{\text{amount of } CH_4 \text{ produced (ppm)}}{\text{amount of photocatalyst used (g)}} \quad (7)$$

Five cycles of CO_2 photoreduction were performed to test the stability of the same sample; after every test, the photoreactor was purged with Ar gas and vacuum, then re-filled with CO_2 gas (1000 ppm in He), followed by a 1 h illumination for the next testing cycle.

4. CONCLUSIONS

In summary, hybrid Cu_xO-TiO_2 photocatalysts are prepared via a facile experimental approach comprising two steps, that is, synthesis of Cu/Cu_2O nanocomposites followed by mixing with $TiCl_4$ and subsequent oxidation. The as-prepared samples are characterized using analytical techniques including XRD, TEM, UV−vis DRS, PL, BET, and XPS. A red shift in the light absorption is observed for the Cu_xO-TiO_2 samples, mainly attributed to the formation of nanoscale heterojunctions between Cu_xO and anatase TiO_2, providing a better charge separation and an increase in the optical absorption. Among the Cu_xO-TiO_2 samples, the sample CT07 produces the highest CH_4 yield with production rates, 11.1 and 22 times higher than pure CuO and TiO_2, respectively. The improved photocatalytic activity can be attributed to (1) the improved light absorption with a significant red shift in the absorption wavelength; (2) formation of p−n heterojunctions with suitable band edge positions for the improved separation of the photogenerated charge; and (3) large surface areas to promote interfacial reactions. A further increase in the $TiCl_4$ amount, sample CT09, resulted in a decrease in the CH_4 evolution rate, which we believe is due to a reduced surface area and a wider bandgap.

Our material synthesis strategy of hybrid Cu_xO-TiO_2 recommends coupling of low-bandgap materials with large-bandgap materials as an efficient approach for the design of high-performance photocatalysts.

■ ASSOCIATED CONTENT

Supporting Information

The Supporting Information is available free of charge on the ACS Publications website at DOI: 10.1021/acsomega.6b00164.

Experimental section for the synthesis of Cu/Cu_2O nanocomposites, schematic experimental setup for the photocatalytic CO_2 conversion test, FE-SEM image of the CT07 sample, HR-TEM image of the CT07 sample, FE-SEM EDS of the CT07 sample, STEM elemental mapping of the CT07 sample, N_2 physisorption isotherms of the hybrid Cu_xO-TiO_2 heterostructured composites, XPS results of the CT03, CT05, and CT09 samples, UV−vis absorption spectra and XRD pattern of the Cu/Cu_2O nanocomposites, and Stability test of the CT07 sample (PDF)

■ AUTHOR INFORMATION

Corresponding Author

*E-mail: insuil@dgist.ac.kr. Phone: +82-53-785-6417. Fax: +82-53-785-6409 (S.-I.I.).

Notes

The authors declare no competing financial interest.

DOI: 10.1021/acsomega.6b00164
ACS Omega 2016, 1, 868−875

■ ACKNOWLEDGMENTS

The authors gratefully acknowledge the support of the DGIST R&D Program of the Ministry of Education, Science and Technology of Korea (16-BD-0404) and the Basic Science research program through the National Research Foundation of Korea funded by the Ministry of Science, ICT and Future Planning (2013R1A1A008678 & 2014K1A3A1A47067086). This research was also supported by the Technology Development Program to Solve Climate Changes of the National Research Foundation (NRF) funded by the Ministry of Science, ICT and Future Planning (2015M1A2A2074670). The authors are thankful to the DGIST R&D Program and the MIREBraiN Program of the Ministry of Science, ICT and Future Planning (15-01-HRSS01 & 201510023).

■ REFERENCES

(1) Hu, B.; Guild, C.; Suib, S. L. Thermal, electrochemical, and photochemical conversion of CO_2 to fuels and value-added products. *J. CO_2 Util.* **2013**, *1*, 18−27.
(2) Maeda, C.; Miyazaki, Y.; Ema, T. Recent progress in catalytic conversions of carbon dioxide. *Catal. Sci. Technol.* **2014**, *4*, 1482−1497.
(3) Linsebigler, A. L.; Yates, J. T., Jr.; Lu, G. Photocatalysis on TiO_2 Surfaces: Principles, Mechanisms, and Selected Results. *Chem. Rev.* **1995**, *95*, 735−758.
(4) Asahi, R.; Morikawa, T.; Ohwaki, T.; Aoki, K.; Taga, Y. Visible-Light Photocatalysis in Nitrogen-Doped Titanium Oxides. *Science* **2001**, *293*, 269−271.
(5) Jiao, J.; Wei, Y.; Zhao, Z.; Zhong, W.; Liu, J.; Li, J.; Duan, A.; Jiang, G. Synthesis of 3D ordered macroporous TiO_2-supported Au nanoparticle photocatalysts and their photocatalytic performances for the reduction of CO_2 to methane. *Catal. Today* **2015**, *258*, 319−326.
(6) Uner, D.; Oymak, M. M. On the mechanism of photocatalytic CO_2 reduction with water in the gas phase. *Catal. Today* **2012**, *181*, 82−88.
(7) Yoon, S.; Kim, M.; Kim, I.-S.; Lim, J.-H.; Yoo, B. Manipulation of cuprous oxide surfaces for improving their photocatalytic activity. *J. Mater. Chem. A* **2014**, *2*, 11621−11627.
(8) Lalitha, K.; Sadanandam, G.; Kumari, V. D.; Subrahmanyam, M.; Sreedhar, B.; Hebalkar, N. Y. Highly stabilized and finely dispersed Cu_2O/TiO_2: A promising visible sensitive photocatalyst for continuous production of hydrogen from glycerol:water mixtures. *J. Phys. Chem. C* **2010**, *114*, 22181−22189.
(9) In, S.-I.; Vaughn, D. D.; Schaak, R. E. Hybrid CuO-$TiO_{2-x}N_x$ hollow nanocubes for photocatalytic conversion of CO_2 into methane under solar irradiation. *Angew. Chem., Int. Ed.* **2012**, *51*, 3915−3918.
(10) Qiu, X.; Miyauchi, M.; Sunada, K.; Minoshima, M.; Liu, M.; Lu, Y.; Li, D.; Shimodaira, Y.; Hosogi, Y.; Kuroda, Y.; et al. Hybrid Cu_xO/TiO_2 nanocomposites as risk-reduction materials in indoor environments. *ACS Nano* **2012**, *6*, 1609−1618.
(11) Wang, P.; Tang, Y.; Wen, X.; Amal, R.; Ng, Y. H. Enhanced Visible Light-Induced Charge Separation and Charge Transport in Cu_2O-Based Photocathodes by Urea Treatment. *ACS Appl. Mater. Interfaces* **2015**, *7*, 19887−19893.
(12) Xu, H.; Ouyang, S.; Liu, L.; Wang, D.; Kako, T.; Ye, J. Porous-structured Cu_2O/TiO_2 nanojunction material toward efficient CO_2 photoreduction. *Nanotechnology* **2014**, *25*, 165402.
(13) Qin, S.; Xin, F.; Liu, Y.; Yin, X.; Ma, W. Photocatalytic reduction of CO_2 in methanol to methyl formate over CuO−TiO_2 composite catalysts. *J. Colloid Interface Sci.* **2011**, *356*, 257−261.
(14) Kumar, D. P.; Shankar, M. V.; Kumari, M. M.; Sadanandam, G.; Srinivas, B.; Durgakumari, V. Nano-size effects on CuO/TiO_2 catalysts for highly efficient H_2 production under solar light irradiation. *Chem. Commun.* **2013**, *49*, 9443−9445.
(15) Luna, A. L.; Valenzuela, M. A.; Colbeau-Justin, C.; Vázquez, P.; Rodriguez, J. L.; Avendaño, J. R.; Alfaro, S.; Tirado, S.; Garduño, A.; De la Rosa, J. M. Photocatalytic degradation of gallic acid over CuO−TiO_2 composites under UV/Vis LEDs irradiation. *Appl. Catal., A* **2016**, *521*, 140−148.
(16) Méndez-Medrano, M. G.; Kowalska, E.; Lehoux, A.; Herissan, A.; Ohtani, B.; Bahena, D.; Briois, V.; Colbeau-Justin, C.; Rodríguez-López, J. L.; Remita, H. Surface Modification of TiO_2 with Ag Nanoparticles and CuO Nanoclusters for Application in Photocatalysis. *J. Phys. Chem. C* **2016**, *120*, 5143−5154.
(17) Xu, H.; Zheng, Z.; Zhang, L.; Zhang, H.; Deng, F. Hierarchical chlorine-doped rutile TiO_2 spherical clusters of nanorods: Large-scale synthesis and high photocatalytic activity. *J. Solid State Chem.* **2008**, *181*, 2516−2522.
(18) Xu, J.; Li, L.; Yan, Y.; Wang, H.; Wang, X.; Fu, X.; Li, G. Synthesis and photoluminescence of well-dispersible anatase TiO_2 nanoparticles. *J. Colloid Interface Sci.* **2008**, *318*, 29−34.
(19) Yousef, A.; Barakat, N. A. M.; Kim, H. Y. Electrospun Cu-doped titania nanofibers for photocatalytic hydrolysis of ammonia borane. *Appl. Catal., A* **2013**, *467*, 98−106.
(20) Dagher, S.; Haik, Y.; Ayesh, A. I.; Tit, N. Synthesis and optical properties of colloidal CuO nanoparticles. *J. Lumin.* **2014**, *151*, 149−154.
(21) Hensel, J.; Wang, G.; Li, Y.; Zhang, J. Z. Synergistic effect of CdSe quantum dot sensitization and nitrogen doping of TiO_2 nanostructures for photoelectrochemical solar hydrogen generation. *Nano Lett.* **2010**, *10*, 478−483.
(22) Huang, Q.; Kang, F.; Liu, H.; Li, Q.; Xiao, X. Highly aligned $Cu_2O/CuO/TiO_2$ core/shell nanowire arrays as photocathodes for water photoelectrolysis. *J. Mater. Chem. A* **2013**, *1*, 2418−2425.
(23) Li, P.; Wang, H.; Xu, J.; Jing, H.; Zhang, J.; Han, H.; Lu, F. Reduction of CO_2 to low carbon alcohols on CuO FCs/Fe_2O_3 NTs catalyst with photoelectric dual catalytic interfaces. *Nanoscale* **2013**, *5*, 11748−11754.
(24) Liu, P.; Li, Z.; Cai, W.; Fang, M.; Luo, X. Fabrication of cuprous oxide nanoparticles by laser ablation in PVP aqueous solution. *RSC Adv.* **2011**, *1*, 847−851.
(25) Kim, K.; Razzaq, A.; Sorcar, S.; Park, Y.; Grimes, C. A.; In, S.-I. Hybrid mesoporous Cu_2ZnSnS_4 (CZTS)−TiO_2 photocatalyst for efficient photocatalytic conversion of CO_2 into CH_4 under solar irradiation. *RSC Adv.* **2016**, *6*, 38964−38971.
(26) Parayil, S. K.; Razzaq, A.; In, S.-I. Formation of titania-silica mixed oxides in solvent mixtures and their influences for the photocatalytic CO_2 conversion to hydrocarbon. *J. Nanosci. Nanotechnol.* **2015**, *15*, 7285−7292.
(27) Razzaq, A.; Grimes, C. A.; In, S.-I. Facile fabrication of a noble metal-free photocatalyst: TiO_2 nanotube arrays covered with reduced graphene oxide. *Carbon* **2016**, *98*, 537−544.
(28) Lee, H.; In, S.; Horn, M. W. Plasmonic enhancement of CO_2 conversion to methane using sculptured copper thin films grown directly on TiO_2. *Thin Solid Films* **2014**, *565*, 105−110.
(29) Zheng, J. Y.; Song, G.; Kim, C. W.; Kang, Y. S. Facile preparation of p-CuO and p-CuO/n-$CuWO_4$ junction thin films and their photoelectrochemical properties. *Electrochim. Acta* **2012**, *69*, 340−344.
(30) Bessekhouad, Y.; Robert, D.; Weber, J.-V. Photocatalytic activity of Cu_2O/TiO_2, Bi_2O_3/TiO_2 and $ZnMn_2O_4/TiO_2$ heterojunctions. *Catal. Today* **2005**, *101*, 315−321.
(31) Ghadimkhani, G.; de Tacconi, N. R.; Chanmanee, W.; Janaky, C.; Rajeshwar, K. Efficient solar photoelectrosynthesis of methanol from carbon dioxide using hybrid CuO−Cu_2O semiconductor nanorod arrays. *Chem. Commun.* **2013**, *49*, 1297−1299.
(32) Indrakanti, V. P.; Kubicki, J. D.; Schobert, H. H. Photoinduced activation of CO_2 on Ti-based heterogeneous catalysts: Current state, chemical physics-based insights and outlook. *Energy Environ. Sci.* **2009**, *2*, 745−758.
(33) Habisreutinger, S. N.; Schmidt-Mende, L.; Stolarczyk, J. K. Photocatalytic reduction of CO_2 on TiO_2 and other semiconductors. *Angew. Chem., Int. Ed.* **2013**, *52*, 7372−7408.
(34) Anpo, M.; Yamashita, H.; Ichihashi, Y.; Ehara, S. Photocatalytic reduction of CO_2 with H_2O on various titanium oxide catalysts. *J. Electroanal. Chem.* **1995**, *396*, 21−26.

DOI: 10.1021/acsomega.6b00164
ACS Omega 2016, 1, 868−875

(35) Shkrob, I. A.; Dimitrijevic, N. M.; Marin, T. W.; He, H.; Zapol, P. Heteroatom-Transfer Coupled Photoreduction and Carbon Dioxide Fixation on Metal Oxides. *J. Phys. Chem. C* **2012**, *116*, 9461−9471.
(36) Koppenol, W. H.; Rush, J. D. Reduction potential of the carbon dioxide/carbon dioxide radical anion: A comparison with other C1 radicals. *J. Phys. Chem.* **1987**, *91*, 4429−4430.
(37) Kortlever, R.; Shen, J.; Schouten, K. J. P.; Calle-Vallejo, F.; Koper, M. T. M. Catalysts and Reaction Pathways for the Electrochemical Reduction of Carbon Dioxide. *J. Phys. Chem. Lett.* **2015**, *6*, 4073−4082.
(38) Poulston, S.; Parlett, P. M.; Stone, P.; Bowker, M. Surface oxidation and reduction of CuO and Cu_2O studied using XPS and XAES. *Surf. Interface Anal.* **1996**, *24*, 811−820.
(39) Wijesundera, R. P. Fabrication of the CuO/Cu_2O heterojunction using an electrodeposition technique for solar cell applications. *Semicond. Sci. Technol.* **2010**, *25*, 45015.
(40) Yu, J.; Hai, Y.; Jaroniec, M. Photocatalytic hydrogen production over CuO-modified titania. *J. Colloid Interface Sci.* **2011**, *357*, 223−228.
(41) Kim, H. R.; Razzaq, A.; Heo, H. J.; In, S.-I. Photocatalytic conversion of CO_2 into hydrocarbon fuels with standard titania (degussa P25) using newly installed experimental setup. *Rapid Commun. Photosci.* **2013**, *2*, 64−66.

DOI: 10.1021/acsomega.6b00164
ACS Omega 2016, 1, 868−875